

Magmatic fluids in melt inclusion-Revision2

1 Revision 2: Detection of liquid H<sub>2</sub>O in vapor bubbles in  
2 reheated melt inclusions: implications for magmatic fluid  
3 composition and volatile budgets of magmas?

4 **Rosario Esposito<sup>1,2\*</sup>, Hector M. Lamadrid<sup>3</sup>, Daniele Redi<sup>4</sup>, Matthew Steele-**  
5 **MacInnis<sup>5</sup>, Robert J. Bodnar<sup>3</sup>, Craig E. Manning<sup>1</sup>, Benedetto De Vivo<sup>2</sup>, Claudia**  
6 **Cannatelli<sup>2,6</sup>, Annamaria Lima<sup>2</sup>**

7 <sup>1</sup>*Earth, Planetary and Space Sciences, UCLA, 595 Charles Young Drive East, Los*  
8 *Angeles, CA 90095-1567, USA*

9 <sup>2</sup>*DISTAR, Università Federico II, Via Mezzocannone 8, Napoli, 80134, Italy*

10 <sup>3</sup>*Department of Geoscience, Virginia Tech, 4044 Derring Hall, Blacksburg VA, 24061*  
11 *USA*

12 <sup>4</sup>*BiGea, Dipartimento di Scienze Biologiche, Geologiche ed Ambientali, Via di Porta San*  
13 *Donato 1, 40126, Bologna, Italy*

14 <sup>5</sup>*Department of Geosciences, University of Arizona, Tucson AZ USA*

15 <sup>6</sup>*Department of Geology and Andean Geothermal Center of Excellence (CEGA),*  
16 *Universidad de Chile, Santiago, Chile*

17

18 **ABSTRACT**

19 Fluids exsolved from mafic melts are thought to be dominantly CO<sub>2</sub>-H<sub>2</sub>O ± S fluids.  
20 Curiously, although CO<sub>2</sub> vapor occurs in bubbles of mafic melt inclusions (MI) at room  
21 temperature (T), the expected accompanying vapor and liquid H<sub>2</sub>O has not been  
22 found. We reheated olivine-hosted MI from Mt. Somma-Vesuvius, Italy and quenched

## Magmatic fluids in melt inclusion-Revision2

23 the MI to a bubble-bearing glassy state. Using Raman spectroscopy, we show that the  
24 volatiles exsolved after quenching include liquid H<sub>2</sub>O at room T and vapor H<sub>2</sub>O at 150°C.  
25 We hypothesize that H<sub>2</sub>O initially present in the MI bubbles was lost to adjacent glass  
26 during local, sub-micron-scale devitrification prior to sample collection. During MI  
27 heating experiments, the H<sub>2</sub>O is redissolved in the vapor in the bubble, where it remains  
28 after quenching, at least on the relatively short time scales of our observations. These  
29 results indicate that (1) a significant amount of H<sub>2</sub>O may be stored in vapor bubble of  
30 bubble-bearing MI and (2) the composition of magmatic fluids directly exsolving from  
31 mafic melts associated the Mt. Somma-Vesuvius may contain up to 29 wt% H<sub>2</sub>O.

32

### 33 **1. Introduction**

34 Melt inclusions (MI) are aliquots of melt trapped in phenocrysts during  
35 crystallization of magmas. MI analyses potentially allow characterization of the volatile  
36 contents of pre-eruptive silicate melts. Typically, concentrations of volatiles such as H<sub>2</sub>O,  
37 CO<sub>2</sub> and S are measured in the glass phase in quenched MI and compared to  
38 experimentally determined solubility models to deduce the composition of a coexisting  
39 vapor phase (Métrich and Wallace 2008 and references therein). However, recent studies  
40 have emphasized that, after entrapment, most of the CO<sub>2</sub> may be transferred from the  
41 melt or glass to a coexisting vapor phase bubble within the MI (e.g., Esposito et al. 2011),  
42 as a result of processes such as post-entrapment crystallization (Steele-MacInnis et al.  
43 2011) or differential thermal contraction (Moore et al. 2015 and references therein). In  
44 fact, bubbles in MI may contain more CO<sub>2</sub> (by mass) than the coexisting glass phase  
45 (Anderson and Brown 1993; Esposito et al. 2011; Hartley et al. 2014; Moore et al. 2015;

## Magmatic fluids in melt inclusion-Revision2

46 Wallace et al. 2015). Thus, it is necessary to understand the partitioning of volatiles  
47 between melt (or glass) and bubbles during MI cooling as part of the characterization of  
48 pre-eruptive volatile systematics (e.g., Kamenetsky et al. 2002; Lowenstern 1995).

49 H<sub>2</sub>O may be abundant in mafic melts and should also be partitioned into any MI  
50 bubbles that form. However, reports of condensed, liquid H<sub>2</sub>O are chiefly in MI hosted  
51 by quartz in plutonic evolved systems (e.g., Frezzotti 2001; Harris et al. 2003; Zajacz et  
52 al. 2008). Several studies have commented on the non-detection of H<sub>2</sub>O in bubbles within  
53 felsic and mafic melt inclusions in volcanic rocks. For instance, Lowenstern et al. (1991)  
54 reported CO<sub>2</sub> vapor in the bubbles of reheated MI hosted in quartz from Pantelleria  
55 (Italy), and stated that H<sub>2</sub>O was likely present in the bubble, but “*the lack of a liquid*  
56 *phase in the bubble and negligible H<sub>2</sub>O vapor peaks in the IR spectra indicated that it*  
57 *was subordinate to CO<sub>2</sub>”*. Yang and Scott (1996) and Kamenetsky et al. (2002 and 2001)  
58 also found that the main volatile component of MI bubbles was CO<sub>2</sub>, and echoed  
59 Lowenstern (1991) in stating that although H<sub>2</sub>O was likely present, it was not detected. It  
60 is important to note that Kamenetsky et al. (2002) detected H<sub>2</sub>O as a component of  
61 gypsum, nahcolite, and silicate crystals found at bubble-glass interfaces. Moore et al.  
62 (2015) suggested that the "missing" H<sub>2</sub>O could reflect nuances of spectroscopic detection  
63 of H<sub>2</sub>O, particularly given that H<sub>2</sub>O-CO<sub>2</sub> fluids would likely separate into an H<sub>2</sub>O-rich  
64 liquid and CO<sub>2</sub>-rich vapor at ambient conditions. Anderson (1991) suggested that H<sub>2</sub>O  
65 could be present in devitrified glass surrounding bubbles.

66 Based on the various results and interpretations described above, H<sub>2</sub>O  
67 is expected to be a major component of magmatic fluids contained in  
68 bubbles that form in MI during cooling, but direct evidence of liquid or

## Magmatic fluids in melt inclusion-Revision2

69 vapor H<sub>2</sub>O in bubbles in olivine-hosted, basaltic MI has not, to our  
70 knowledge, been reported. In this study, we hypothesized that liquid H<sub>2</sub>O may be  
71 recognized in very "fresh" bubbles generated by laboratory re-heating and quenching of  
72 MI. Naturally glassy MI were heated to conditions at which the silicate component of the  
73 MI was fully molten. With subsequent quenching, a glass and bubble would be produced,  
74 and liquid H<sub>2</sub>O in the bubble, if present, could be detected because it would have little  
75 time to interact with the surrounding glass.

76

### 77 **2. Materials and Methods**

78 Sixteen olivine phenocrysts were selected from lavas and pumices produced during  
79 mild effusive events and explosive Plinian eruptions of Mt. Somma-Vesuvius between  
80 >33 ka and AD 1631 ([Supplement A](#)). Bulk-rock compositions of the samples studied  
81 span a wide range, and correspond to samples reported by Ayuso et al. (1998). Lava  
82 samples are slightly Si-undersaturated and plot at the boundary between the  
83 trachybasalt/shoshonite fields on the TAS diagram (Le Bas et al. 1986). Pumice samples  
84 show a higher degree of Si undersaturation and plot in the phonotephrite, tephriphonolite  
85 and phonolite fields. The olivines selected for this study span in a wide compositional  
86 range from 68 to 90 mole% forsterite (Redi 2014). We identified MI based on  
87 petrographic analysis. Particular care was taken to select MI not showing decrepitation or  
88 fractures intersecting the MI. We performed heating experiments using a Vernadsky  
89 heating stage (Sobolev et al. 1980). The average duration of the heating experiments was  
90 17 minutes ([Supplement B](#)), but MI were not heated for more than 9 minutes at T  
91 >800°C. The 16 phenocrysts contained bubble-bearing MI after quenching from

## Magmatic fluids in melt inclusion-Revision2

92 the maximum T (1143~ 1238°C; [Fig. 1](#) and [Table DR1](#)). After rapid quenching, the  
93 bubbles were examined for evidence of volatile components (CO<sub>2</sub>, H<sub>2</sub>O, etc.) in the  
94 exsolved magmatic fluid. The MI were analyzed by Raman spectroscopy ([Supplement](#)  
95 [B](#)). The Raman signal corresponding to hydroxyl ions and molecular H<sub>2</sub>O (H<sub>2</sub>O/OH)  
96 dissolved in the glass ([Fig. 2 and 3](#)) is clearly discernable from the signals of both H<sub>2</sub>O  
97 liquid at the glass/bubble interface ([Fig. 3](#)) and the H<sub>2</sub>O in the H<sub>2</sub>O-CO<sub>2</sub> vapor phase at  
98 >100°C. The density of CO<sub>2</sub> in the vapor phase was calculated from the splitting of the  
99 CO<sub>2</sub> Fermi diad ([Supplement B](#)).

100 Some vapor bubbles were analyzed by Raman spectroscopy at high T (up to 150°C)  
101 to test for the presence of H<sub>2</sub>O in the bubbles ([Supplement B](#)). To estimate concentrations  
102 of H<sub>2</sub>O and CO<sub>2</sub> in the magmatic vapor phase, we compared the relative peak areas of  
103 H<sub>2</sub>O and CO<sub>2</sub> in the spectra acquired at 150 °C ([Supplement B](#)). In addition, five  
104 freezing/heating experiments were performed on MI bubbles ([Supplement B](#)).

105

### 106 **3. Results**

107 Twenty MI selected for this study were examined petrographically before, during,  
108 and after the heating experiments ([Table DR1](#)). MI varied from slightly crystallized to  
109 highly crystallized (e.g., [Fig. 1](#)). Details of the microthermometric behavior of MI are  
110 reported in [Supplement C](#). We did not heat the MI until the bubble was completely  
111 dissolved, because our aim was to quench a vapor bubble in thermal equilibrium with  
112 a silicate melt at maximum T to study its vapor constituents. The olivine phenocrysts  
113 were held at maximum T (1143-1238°C) for ~ 3 minutes to attain thermal equilibrium.

## Magmatic fluids in melt inclusion-Revision2

114 Immediately prior to quenching, the MI contained silicate liquid plus a minute vapor  
115 bubble. Upon quenching, the MI contained glass plus a bubble.

116       When the laser beam was focused in the center of the bubble, CO<sub>2</sub> was detected in  
117 all cases. The density of CO<sub>2</sub> ranged from 0.04 to 0.14 g/cm<sup>3</sup> with one outlier ([Table](#)  
118 [DR1](#)). No H<sub>2</sub>O was detected in the vapor at room T. The bubbles were also analyzed at  
119 the glass-bubble interface. At the upper interface, sub-hexagonal crystals and dark flakes  
120 of calcite (in 4 bubbles) or calcite plus native sulfur (in 3 bubbles) were observed and  
121 analyzed ([Fig. 2b](#); [Table DR1](#)). We did not observe these crystal aggregates at high T.  
122 We also detected gypsum at the glass/bubble interface of one vapor bubble (P1-D49-2-7;  
123 [Fig. C1](#) and [Table DR1](#)). After focusing on the calcite ± native sulfur aggregates, the  
124 laser was focused ~1 μm below or beside the crystalline aggregates ([Fig. 2](#)). At this  
125 position, five MI also showed evidence of liquid H<sub>2</sub>O at the glass-bubble interface ([Table](#)  
126 [DR1](#)). Some Raman spectra at the glass-bubble interface indicated the coexistence of  
127 carbonates ± native sulfur, H<sub>2</sub>O, and CO<sub>2</sub> ([Fig. 2a](#)). In six H<sub>2</sub>O-bearing MI, the presence  
128 of H<sub>2</sub>O and CO<sub>2</sub> was confirmed by microthermometry. Five bubble-bearing MI analyzed  
129 by microthermometry showed first melting ranging from -57.1 to -56.0°C ([Table DR1](#)),  
130 close to the triple point of CO<sub>2</sub> (-56.6°C), suggesting that the vapor is nearly pure CO<sub>2</sub>. A  
131 second phase change was observed at -2°C to +8°C in four out of the five bubbles, likely  
132 representing melting of H<sub>2</sub>O-ice or CO<sub>2</sub>-H<sub>2</sub>O clathrate.

133       Three H<sub>2</sub>O-bearing samples were heated to 150°C after quenching. At this  
134 temperature, liquid H<sub>2</sub>O was no longer observed and the vapor in the bubbles showed the  
135 sharp O-H stretching band of H<sub>2</sub>O vapor (Frezzotti et al., 2012) at ~3647 cm<sup>-1</sup> ([Fig. 3](#)).  
136 This indicates that the H<sub>2</sub>O occurring as liquid at room T had dissolved into the CO<sub>2</sub>-rich

## Magmatic fluids in melt inclusion-Revision2

137 vapor phase at higher T.

138 The molar fractions of H<sub>2</sub>O and CO<sub>2</sub> were estimated from the relative Raman peak  
139 areas, normalized according to the relative scattering efficiencies (Burke 2001). For  
140 inclusion LFL2-D44-3-2 (Avellino eruption), two analyses at two focal depths within the  
141 bubble yielded H<sub>2</sub>O concentrations of 20 ±12 mol% and 30 ±21 mol% H<sub>2</sub>O.

142

### 143 **4. Discussion and implications**

144 Bubbles in MI may contain significant proportions of the total CO<sub>2</sub> in the inclusions  
145 (Anderson and Brown 1993; Esposito et al. 2011; Hartley et al. 2014; Moore et al. 2015;  
146 Wallace et al. 2015), but evidence for the expected H<sub>2</sub>O has been hitherto lacking. Our  
147 results demonstrate that bubbles in reheated MI from Mt. Somma-Vesuvius show  
148 evidence of H<sub>2</sub>O and S, in addition to CO<sub>2</sub>. At ambient T, H<sub>2</sub>O is present as a thin liquid  
149 film at the bubble-glass interface, and S is present in minute daughter crystals. The  
150 presence of H<sub>2</sub>O in reheated bubbles raises the possibility that the bubble volatile phase  
151 may initially have been H<sub>2</sub>O rich.

152 Based on the Raman spectroscopic data and constraints from previous studies  
153 (Belkin and De Vivo 1993; Marianelli et al. 2005), we estimated that the thickness of the  
154 liquid H<sub>2</sub>O film contained in the MI bubbles ranges from ~0.01 to 0.51 μm and, thus, in  
155 all cases, the liquid H<sub>2</sub>O annulus would be optically undetectable (see [Supplement D](#),  
156 [Table DR2](#)). In this study we did not attempt to establish the bulk H<sub>2</sub>O content of the MI,  
157 but previous results can be used as a guide.

158 Sample MI SCL14-D92-3-1 (Fig. 2) is representative of lava samples studied by  
159 Webster et al. (2001). If we assume that the concentration of H<sub>2</sub>O ranges from 20 to 60

## Magmatic fluids in melt inclusion-Revision2

160 mole%, the thickness of liquid H<sub>2</sub>O film at the glass/bubble interface of MI SCL14-D92-  
161 3-1 is 0.04-0.23 μm (Table DR2). The amount of H<sub>2</sub>O stored in this bubble represents  
162 between 3 and 16% of the total amount of H<sub>2</sub>O in the melt that was trapped in the MI if  
163 we assume that the H<sub>2</sub>O content of the original trapped melt is 0.3 wt%, consistent with  
164 the lowest H<sub>2</sub>O content reported by Webster et al. (2001, see their Table 1). Webster et al.  
165 (2001) give an upper bound of 5 wt% H<sub>2</sub>O. Assuming this value, the amount of H<sub>2</sub>O  
166 stored in the bubble of this MI is insignificant, and is the reason for the query in the title  
167 of this letter. In general, the amount of H<sub>2</sub>O in the bubbles of bubble-bearing MI may be  
168 significant for (1) relatively low H<sub>2</sub>O concentration of the originally trapped melt, (2)  
169 relatively high mole% H<sub>2</sub>O in the fluid, (3) relatively large vapor bubbles, and (4) at  
170 constant bubble volume%, relatively small bubble-bearing MI. As an example, a bubble  
171 with 85 mole% H<sub>2</sub>O, condensed as a liquid H<sub>2</sub>O film that is 1 μm thick (thus not optically  
172 recognizable) assuming CO<sub>2</sub> density is 0.14 g/cm<sup>3</sup>. The H<sub>2</sub>O in the bubble would  
173 represent 59% of the total H<sub>2</sub>O in the MI if the glass H<sub>2</sub>O concentration is 0.3 wt%  
174 assuming the bubble is 3 volume%.

175       The likely reason that H<sub>2</sub>O has been overlooked is that in most MI, the H<sub>2</sub>O  
176 originally in the vapor bubble is now incorporated in the surrounding glass phase via  
177 hydration (Anderson 1991; Parruzot et al. 2015). Devitrification and alteration of silicate  
178 glass in the presence of H<sub>2</sub>O is a relatively fast process [ $\sim 10^3$  years at ambient T (Lee et  
179 al. 1974),  $\sim$ days at  $>200^\circ\text{C}$  (Mazer et al. 1991)]. Thus, H<sub>2</sub>O liquid would only be detected  
180 in vapor bubbles if the H<sub>2</sub>O re-dissolves into the bubble when the MI is re-heated and  
181 then quenched. Even if the H<sub>2</sub>O component was not incorporated into the glass via  
182 devitrification, it is unlikely that the thin film of liquid H<sub>2</sub>O at the glass/bubble interface



## Magmatic fluids in melt inclusion-Revision2

183 would be discernible because the resolution with an optical microscope is on the order of  
184 1  $\mu\text{m}$ , and the rims may be  $\ll 1 \mu\text{m}$  ([Supplement D and Table DR2](#)). In these cases, it is  
185 important to investigate the glass/bubble interface for liquid  $\pm$  solid(s). These  
186 interpretations are consistent with preliminary indications of  $\text{H}_2\text{O}$  liquid in shrinkage  
187 bubbles of olivine hosted MI from the San Cristóbal volcano in the Central American  
188 Volcanic Arc (Robidoux et al. 2015).

189 The results of this study also provide direct evidence of native S, in addition to  
190  $\text{H}_2\text{O}$ ,  $\text{CO}_2$ , carbonates, and sulfates in vapor bubbles in MI. The presence of S in the  
191 vapor bubble underscores the possibility that the original S concentration of the melt  
192 would be underestimated if only the S contained in the glass is considered. We estimate  
193 that the S in the bubbles ranges from 108 to 1192 ppm, comparable to the concentration  
194 of S reported by Webster et al. (2001), which ranged from 200 to 2900 ppm. Our  
195 calculation assumed that crystals at the glass-bubble interface are a mixture of calcite and  
196 native sulfur of various proportions, and that the  $\text{H}_2\text{O}/\text{CO}_2$  molar ratio ranges from 0.25  
197 to 1.5, and that these crystals are from 1 to 2  $\mu\text{m}$  thick ([Supplement D](#)). Thus, including  
198 the contribution of S in the bubble to the total S content of the MI could more accurately  
199 estimate the pre-eruptive S concentration of silicate melts if the melt was originally  
200 trapped as single melt phase. We estimate that the composition of the C-O-H-S magmatic  
201 fluid exsolving from the mafic melts in this study is 32-89 wt%  $\text{CO}_2$ , 3-29 wt%  $\text{H}_2\text{O}$ , and  
202 6-59 wt% S ([Table 1](#); see [Supplement D](#) for calculations).

203 An important consideration when evaluating the role of bubbles in the volatile  
204 contents of MI will be open system effects, such as hydrogen loss. Hydrogen loss during  
205 heating experiments may not significantly change the  $\text{H}_2\text{O}$  content of a MI if the

## Magmatic fluids in melt inclusion-Revision2

206 experiment is in the order of few minutes (Bucholz et al. 2013; Gaetani et al. 2012). The  
207 maximum time that the MI studied were held at  $T > 800^{\circ}\text{C}$  is 9 minutes. We calculated  
208 that change in the  $\text{H}_2\text{O}$  content of the MI during the experiments is  $< 0.1$  wt% if the  
209 starting  $\text{H}_2\text{O}$  concentration of MI was 4 wt% (see Supplement E for more details).  
210 However, it is possible that H and Fe loss by diffusion occurred after trapping and before  
211 eruption (Danyushevsky et al. 2002) because the history of the MI from trapping to  
212 eruption is unknown.

213 In this study, we cannot establish if the melt inclusions were originally trapped as  
214 volatile-saturated or volatile-unsaturated melts, nor do we know whether bubbles were  
215 present at the time of MI trapping or formed later. We emphasize that the goal of this  
216 study was not to investigate the trapping conditions of the MI and the original magmatic  
217 vapor potentially trapped in the MI. Our goal was instead to use the MI as a natural  
218 laboratory where we were able to form a vapor bubble at magmatic T in thermal  
219 equilibrium with a silicate melt. The observation that reheated and quenched MI contain a  
220 silicate glass plus a fluid bubble indicates that a magmatic vapor phase exsolved from and  
221 coexisted with the melt prior to laboratory quenching because MI studied show a single  
222 bubble at maximum T before quenching. The bubbles in the MI investigated in the  
223 present study represent a magmatic volatile phase that exsolved from and was in  
224 equilibrium with silicate melt at temperatures and pressures appropriate for sub-volcanic  
225 environments, assuming that the bubbles did not lose or gain volatiles during quenching.  
226 At this stage, we cannot rule out possible modifications to the MI after trapping (e.g., H-  
227 loss). Thus, the volatiles in the vapor bubbles could be representative of the magmatic  
228 fluid coexisting with the melt beneath Mt. Somma-Vesuvius only *if* the MI trapped a

## Magmatic fluids in melt inclusion-Revision2

229 volatile-saturated melt, the composition of the MI is unmodified, and the temperatures  
230 (and internal pressures in the inclusions) attained during heating experiments correspond  
231 to the MI trapping conditions. Violation of any of the above criteria would imply that the  
232 MI bubbles do not represent the magmatic vapor phase specific to Mt. Somma-Vesuvius.

233       Regardless of their origin, our results show that bubbles in MI should be carefully  
234 taken into account in any assessment of the volatile concentrations of MI in some  
235 magmatic systems. The direct detection of liquid H<sub>2</sub>O in vapor bubbles in MI has several  
236 potential implications concerning magmatic fluids. For instance, the newly formed vapor  
237 bubbles in MI allow us to investigate the composition of the magmatic fluid directly  
238 exsolving from a natural melt. Raman analysis, coupled with freezing and heating  
239 studies, can be applied to investigate the volatile species and the composition of  
240 magmatic fluids. Also, one could investigate the rate at which the liquid H<sub>2</sub>O reacts with  
241 the surrounding glass by conducting time-resolved Raman imaging analysis (e.g., Bartoli  
242 et al. 2013) at the glass/bubble interface following the formation of vapor bubbles during  
243 cooling of MI in the laboratory.

244

### 245 **ACKNOWLEDGEMENTS**

246 This work was supported by the 7/PON/ST/2012-4 Enerbiochem project to B. De Vivo.  
247 Partial funding for MI analysis was provided by PRIN2010PMKZX7 to C. Cannatelli. R.  
248 Esposito thanks E. Ammannito for discussions on peak fitting of the Raman spectra, and  
249 D. Moncada for help during heating/freezing experiments and Raman analysis at Virginia  
250 Tech. Funding was provided in part by the National Science Foundation (Grant Nos.  
251 EAR-1019770 Bodnar; EAR-1347987; Manning) and the Deep Carbon Observatory. We

## Magmatic fluids in melt inclusion-Revision2

252 thank L. Danyushevsky for critical comments and help with heating experiments. We  
253 thank three anonymous reviewers for critical comments on an earlier version of this  
254 manuscript, A. J. Anderson, C. Bucholz, and M. L. Frezzotti for valuable comments that  
255 helped to improve this letter, and I. Swanson for editorial handling of this manuscript.

256

### 257 **References cited**

- 258 Anderson, A.T., Jr. (1991) Hourglass inclusions: theory and application to the Bishop  
259 Rhyolitic Tuff. *American Mineralogist*, 76, 530-547.
- 260 Anderson, A.T., Jr., and Brown, G.G. (1993) CO<sub>2</sub> contents and formation pressures of  
261 some Kilauean melt inclusions. *American Mineralogist*, 78, 794-803.
- 262 Ayuso, R.A., De Vivo, B., Rolandi, G., Seal II, R.R., and Paone, A. (1998) Geochemical  
263 and isotopic (Nd–Pb–Sr–O) variations bearing on the genesis of volcanic  
264 rocks from Vesuvius, Italy. *Journal of Volcanology and Geothermal  
265 Research*, 82, 53-78.
- 266 Bartoli, O., Cesare, B., Poli, S., Bodnar, R.J., Acosta-Vigil, A., Frezzotti, M.L., and Meli,  
267 S. (2013) Recovering the composition of melt and the fluid regime at the  
268 onset of crustal anatexis and S-type granite formation. *Geology*, 41, 115-  
269 118.
- 270 Belkin, H.E., and De Vivo, B. (1993) Fluid inclusion studies of ejected nodules from  
271 plinian eruptions of Mt. Somma-Vesuvius. *Journal of Volcanology and  
272 Geothermal Research*, 58, 89-100.
- 273 Bucholz, C.E., Gaetani, G.A., Behn, M.D., and Shimizu, N. (2013) Post-entrapment  
274 modification of volatiles and oxygen fugacity in olivine-hosted melt  
275 inclusions. *Earth and Planetary Science Letters*, 374, 145-155.
- 276 Burke, E.A. (2001) Raman microspectrometry of fluid inclusions. *Lithos*, 55, 139-158.
- 277 Danyushevsky, L.V., McNeill, A.W., and Sobolev, A.V. (2002) Experimental and  
278 petrological studies of melt inclusions in phenocrysts from mantle-derived  
279 magmas: an overview of techniques, advantages and complications.  
280 *Chemical Geology*, 183, 5-24.
- 281 Esposito, R., Bodnar, R.J., Danyushevsky, L., De Vivo, B., Fedele, L., Hunter, J., Lima,  
282 A., and Shimizu, N. (2011) Volatile Evolution of Magma Associated with  
283 the Solchiaro Eruption in the Phlegrean Volcanic District (Italy). *Journal  
284 of Petrology*, 52, 2431-2460.
- 285 Frezzotti, M.-L. (2001) Silicate-melt inclusions in magmatic rocks: applications to  
286 petrology. *Lithos*, 55, 273-299.
- 287 Frezzotti, M.L., Tecce, F., and Casagli, A. (2012) Raman spectroscopy for fluid inclusion  
288 analysis. *Journal of Geochemical Exploration*, 112, 1-20.
- 289 Gaetani, G.A., O’Leary, J.A., Shimizu, N., Bucholz, C.E., and Newville, M. (2012)  
290 Rapid reequilibration of H<sub>2</sub>O and oxygen fugacity in olivine-hosted melt  
291 inclusions. *Geology*, 40, 915-918.

## Magmatic fluids in melt inclusion-Revision2

- 292 Harris, A.C., Kamenetsky, V.S., White, N.C., van Achterbergh, E., and Ryan, C.G.  
293 (2003) Melt inclusions in veins: linking magmas and porphyry Cu  
294 deposits. *Science*, 302, 2109-2111.
- 295 Hartley, M.E., Maclennan, J., Edmonds, M., and Thordarson, T. (2014) Reconstructing  
296 the deep CO<sub>2</sub> degassing behaviour of large basaltic fissure eruptions. *Earth  
297 and Planetary Science Letters*, 393, 120-131.
- 298 Kamenetsky, V., Davidson, P., Mernagh, T., Crawford, A., Gemmell, J., Portnyagin, M.,  
299 and Shinjo, R. (2002) Fluid bubbles in melt inclusions and pillow-rim  
300 glasses: high-temperature precursors to hydrothermal fluids? *Chemical  
301 Geology*, 183, 349-364.
- 302 Kamenetsky, V.S., Binns, R.A., Gemmell, J.B., Crawford, A.J., Mernagh, T.P., Maas, R.,  
303 and Steele, D. (2001) Parental basaltic melts and fluids in eastern Manus  
304 backarc Basin: implications for hydrothermal mineralisation. *Earth and  
305 Planetary Science Letters*, 184, 685-702.
- 306 Le Bas, M.J., Le Maitre, R.W., Streckeisen, A., and Zanettin, B.A. (1986) Chemical  
307 classification of volcanic rocks based on the total alkali-silica diagram.  
308 *Journal of Petrology*, 27(3), 745-750.
- 309 Lee, R., Leich, D., and Tombrello, T. (1974) Obsidian hydration profile measurements  
310 using a nuclear reaction technique. *Nature*, 250, 44-47.
- 311 Lowenstern, J.B. (1995) Applications of silicate-melt inclusions to the study of magmatic  
312 volatiles. *Short Course Handbook*, 23, 71-99.
- 313 Lowenstern, J.B., Mahood, G.A., Rivers, M.L., and Sutton, S.R. (1991) Evidence for  
314 extreme partitioning of copper into a magmatic vapor phase. *Science*, 252,  
315 1405-1409.
- 316 Marianelli, P., Sbrana, A., Métrich, N., and Cecchetti, A. (2005) The deep feeding system  
317 of Vesuvius involved in recent violent strombolian eruptions. *Geophysical  
318 Research Letters*, 32, L02306.
- 319 Mazer, J., Bates, J., Stevenson, C., and Bradley, J. (1991) The effect of glass composition  
320 on the experimental hydration of obsidian between 110 and 230 °C.  
321 Argonne National Lab., IL (United States).
- 322 Métrich, N., and Wallace, P.J. (2008) Volatile abundances in basaltic magmas and their  
323 degassing paths tracked by melt inclusions. *Reviews in Mineralogy and  
324 Geochemistry*, 69, 363-402.
- 325 Moore, L., Gazel, E., Tuohy, R., Lloyd, A., Esposito R., Steele-MacInnis, M.J., Hauri,  
326 E.H., Wallace, P., Plank, T., and Bodnar, R.J. (2015) Bubbles matter: An  
327 assessment of the contribution of vapor bubbles to melt inclusion volatile  
328 budgets *American Mineralogist*, 100, 806-823.
- 329 Parruzot, B., Jollivet, P., Rébiscoul, D., and Gin, S. (2015) Long-term alteration of  
330 basaltic glass: Mechanisms and rates. *Geochimica et Cosmochimica Acta*,  
331 154, 28-48.
- 332 Redi, D. (2014) Pyroxene and olivine chemistry as an indicator of melt evolution. A  
333 contribution to the understanding of Somma-Vesuvius eruptive behaviour,  
334 PhD. University of Tasmania and University of Napoli Federico II.
- 335 Robidoux, P., Frezzotti, M.L., Hauri, E.H., and Aiuppa, A. (2015) Low-temperature  
336 superficial chemical changes and post-entrapment effects alter CO<sub>2</sub>

## Magmatic fluids in melt inclusion-Revision2

- 337 budget estimation in vapor bubbles of glass inclusions. AGU Meeting  
 338 2015, San Francisco, United States.  
 339 Sobolev, A.V., Dmitriev, L.V., Barsukov, V.L., Nevsorov, V.N., and Slutsky, A.B.  
 340 (1980) The formation conditions of the high magnesium olivines from the  
 341 monomineralic fraction of Luna 24 regolith. Proceedings of the Lunar and  
 342 Planetary Science Conference, 11, 105-116.  
 343 Steele-MacInnis, M.J., Esposito, R., and Bodnar, R.J. (2011) Thermodynamic model for  
 344 the effect of post-entrapment crystallization on the H<sub>2</sub>O-CO<sub>2</sub> systematics  
 345 of volatile saturated silicate melt inclusions. *Journal of Petrology*, 52,  
 346 2461-2482.  
 347 Wallace, P.J., Kamenetsky, V.S., and Cervantes, P. (2015) Melt inclusion CO<sub>2</sub> contents,  
 348 pressures of olivine crystallization, and the problem of shrinkage bubbles.  
 349 *American Mineralogist*, 100, 787-794.  
 350 Webster, J., Raia, F., De Vivo, B., and Rolandi, G. (2001) The behavior of chlorine and  
 351 sulfur during differentiation of the Mt. Somma-Vesuvius magmatic  
 352 system. *Mineralogy and Petrology*, 73, 177-200.  
 353 Yang, K., and Scott, S.D. (1996) Possible contribution of a metal-rich magmatic fluid to a  
 354 sea-floor hydrothermal system. *Nature*, 383, 420-423.  
 355 Zajacz, Z., Halter, W.E., Pettke, T., and Guillong, M. (2008) Determination of fluid/melt  
 356 partition coefficients by LA-ICPMS analysis of co-existing fluid and  
 357 silicate melt inclusions: controls on element partitioning. *Geochimica et*  
 358 *Cosmochimica Acta*, 72, 2169-2197.  
 359  
 360

361 **Table 1.** Volatile budget of bubbles in MI (see text and [Supplements D](#) for calculations).

| MI                            | SCL14-D92-<br>3-1                   | SCL14-D92-<br>3-1 | LFL2-D44-<br>1-1 | LFL2-D44-<br>1-1 | P1-<br>D492-7 | P1-<br>D492-7 | R6-D54-<br>4-2 | R6-D54-<br>4-2 |
|-------------------------------|-------------------------------------|-------------------|------------------|------------------|---------------|---------------|----------------|----------------|
| Eruption                      | Pre-Codola                          | Pre-Codola        | Avellino         | Avellino         | Pompeii       | Pompeii       | AD 1631        | AD 1632        |
|                               | Mass relative to total MI (ppm)     |                   |                  |                  |               |               |                |                |
|                               | min                                 | max               | min              | max              | min           | max           | min            | max            |
| CO <sub>2</sub> vapor         | 774                                 | 774               | 788              | 788              | 380           | 380           | 330            | 330            |
| CO <sub>2</sub> calcite       | 74                                  | 662               | 79               | 969              | 0             | 0             | 94             | 342            |
| H <sub>2</sub> O liquid       | 77                                  | 464               | 81               | 483              | 121           | 242           | 34             | 210            |
| Native S                      | 124                                 | 1116              | 132              | 1192             | 0             | 0             | 64             | 576            |
| Gypsum S                      | 0                                   | 0                 | 0                | 0                | 108           | 216           | 0              | 0              |
| total                         | 1049                                | 3016              | 1080             | 3432             | 609           | 838           | 522            | 1458           |
|                               | Mass relative to vapor bubble (wt%) |                   |                  |                  |               |               |                |                |
| Magmatic fluid<br>composition | min                                 | max               | min              | max              | min           | max           | min            | max            |
| CO <sub>2</sub> wt%           | 35                                  | 88                | 34               | 89               | 45            | 45            | 32             | 87             |
| H <sub>2</sub> O wt%          | 4                                   | 27                | 4                | 27               | 20            | 29            | 3              | 26             |
| S wt%                         | 6                                   | 55                | 6                | 56               | 18            | 26            | 7              | 59             |

362

## 363 **FIGURE AND CAPTIONS**

## Magmatic fluids in melt inclusion-Revision2

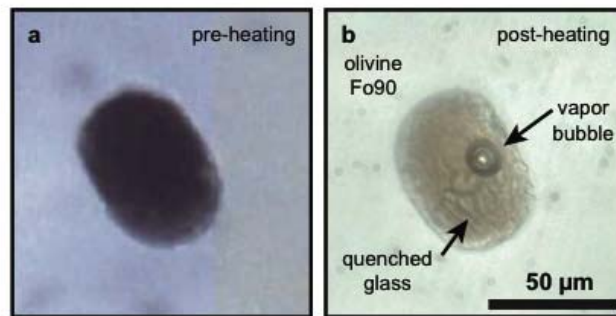


Fig. 1

364

365 Fig. 1 Photomicrographs of MI hosted in olivine from the Pompeii eruption (AD 79). **a**,  
366 Crystallized MI “as found” (before heating experiment). **b**, Bubble-bearing MI after  
367 quenching following heating experiment.

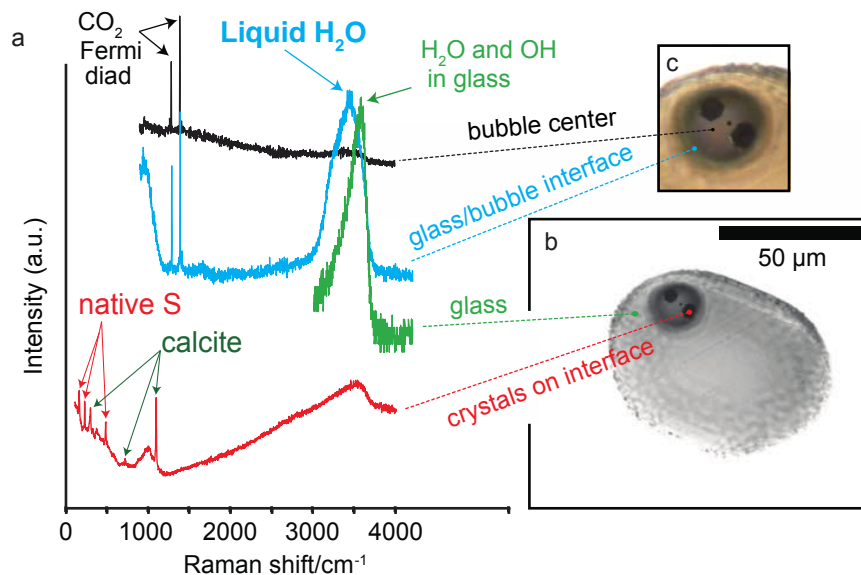


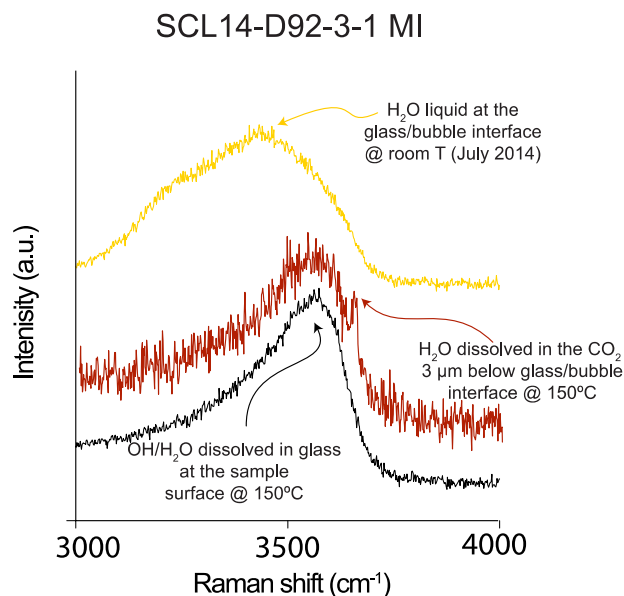
Fig. 2

368

369 Fig. 2 Raman analyses of MI hosted in olivine SCL14-D92-3-1 from a Pre-Codola (>33  
370 ka) lava. **A**, Raman spectra obtained at different depths and position in the MI. Note the  
371 variation in H<sub>2</sub>O peak intensity at the various depths (a.u. = arbitrary units). **B**,

## Magmatic fluids in melt inclusion-Revision2

372 Photomicrograph of the MI showing the hexagonally shaped, dark solids at the  
373 glass/bubble interface. C, Enlargement of the bubble in B.



374  
375 **Fig. 3** Raman spectra collected from the vapor bubble in MI SCL14-D92-3-1 at different  
376 conditions and depths. The yellow spectrum was collected from the MI at room  
377 temperature while focusing the laser at the glass/bubble interface in July 2014 and shows  
378 the H<sub>2</sub>O fluid band. The black spectrum was collected at 150 °C while focusing the laser  
379 in the glass in the MI and shows the OH and H<sub>2</sub>O band at ~3550 cm<sup>-1</sup>. Note the  
380 difference between the peak positions of liquid H<sub>2</sub>O in the synthetic fluid inclusion and at  
381 the glass/bubble interface and those of hydroxyl and molecular water dissolved in the  
382 silicate glass. The red spectrum represents the H<sub>2</sub>O band collected at 150 °C while  
383 focusing the laser at the glass/bubble interface in the MI. Notice that the H<sub>2</sub>O band of  
384 liquid water was not observed at 150 °C, while a peak at ~1650 cm<sup>-1</sup> was only detected  
385 at this temperature (a.u. = arbitrary units).



| MI                                  | SCL14-D92-3-1 | SCL14-D92-3-1 | LFL2-D44-1-1 | LFL2-D44-1-1 | P1-D492-7 | P1-D492-7 | R6-D54-4-2 | R6-D54-4-2 |
|-------------------------------------|---------------|---------------|--------------|--------------|-----------|-----------|------------|------------|
| Eruption                            | Pre-Codola    | Pre-Codola    | Avellino     | Avellino     | Pompeii   | Pompeii   | AD 1631    | AD 1632    |
| Mass relative to total MI (ppm)     |               |               |              |              |           |           |            |            |
|                                     | min           | max           | min          | max          | min       | max       | min        | max        |
| CO <sub>2</sub> vapor               | 774           | 774           | 788          | 788          | 380       | 380       | 330        | 330        |
| CO <sub>2</sub> calcite             | 74            | 662           | 79           | 969          | 0         | 0         | 94         | 342        |
| H <sub>2</sub> O liquid             | 77            | 464           | 81           | 483          | 121       | 242       | 34         | 210        |
| Native S                            | 124           | 1116          | 132          | 1192         | 0         | 0         | 64         | 576        |
| Gypsum S                            | 0             | 0             | 0            | 0            | 108       | 216       | 0          | 0          |
| total                               | 1049          | 3016          | 1080         | 3432         | 609       | 838       | 522        | 1458       |
| Mass relative to vapor bubble (wt%) |               |               |              |              |           |           |            |            |
| Magmatic fluid composition          | min           | max           | min          | max          | min       | max       | min        | max        |
| CO <sub>2</sub> wt%                 | 35            | 88            | 34           | 89           | 45        | 45        | 32         | 87         |
| H <sub>2</sub> O wt%                | 4             | 27            | 4            | 27           | 20        | 29        | 3          | 26         |
| S wt%                               | 6             | 55            | 6            | 56           | 18        | 26        | 7          | 59         |

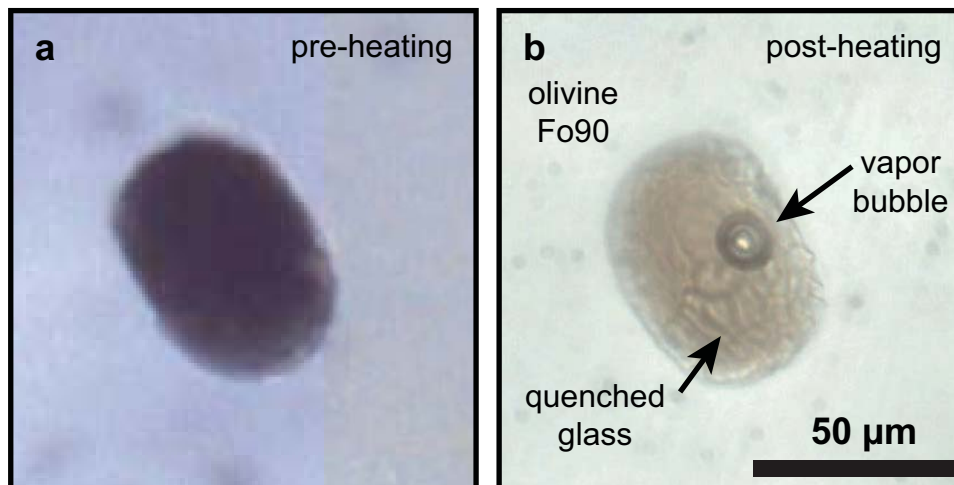


Fig. 1

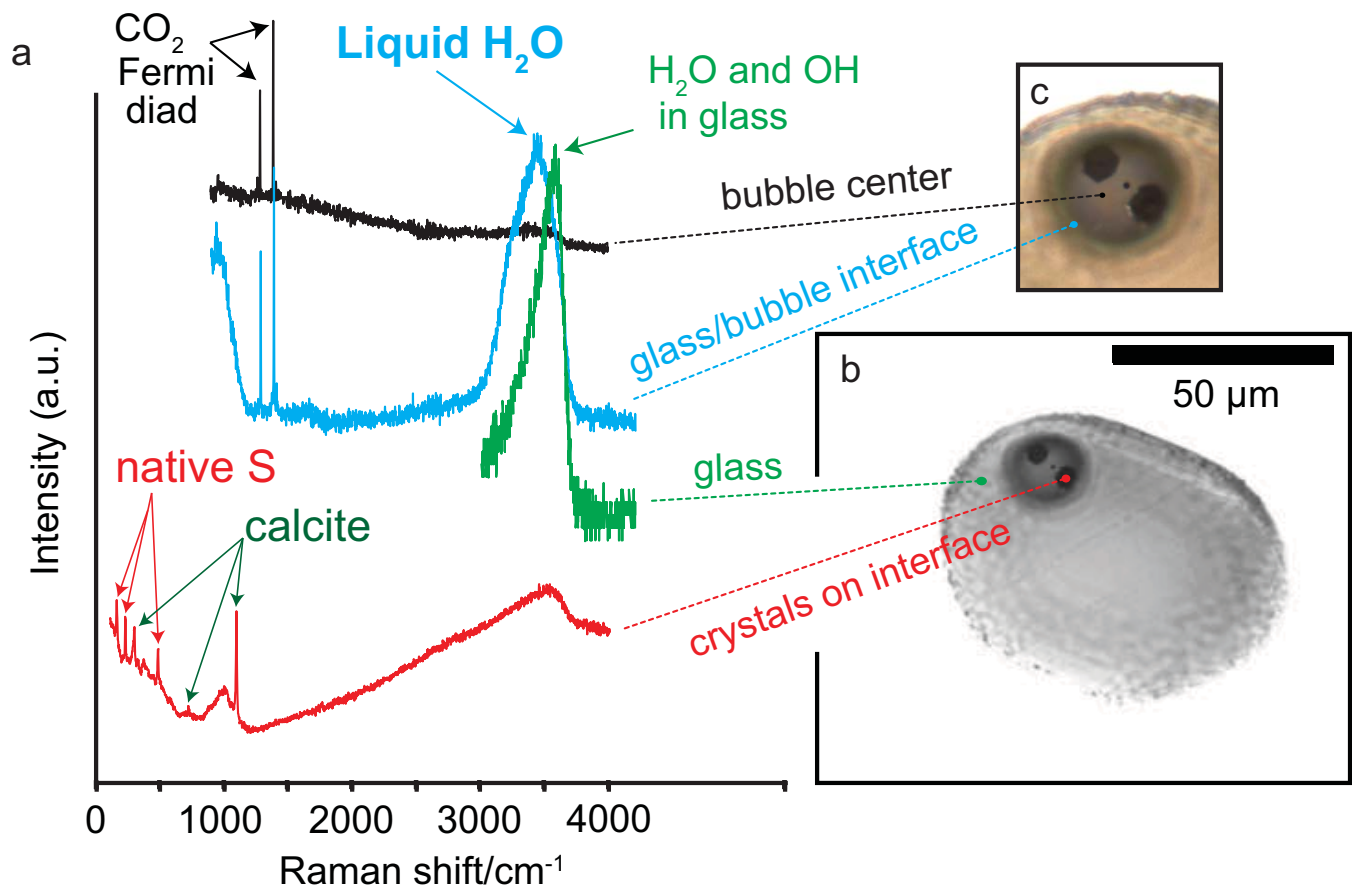


Fig. 2

## SCL14-D92-3-1 MI

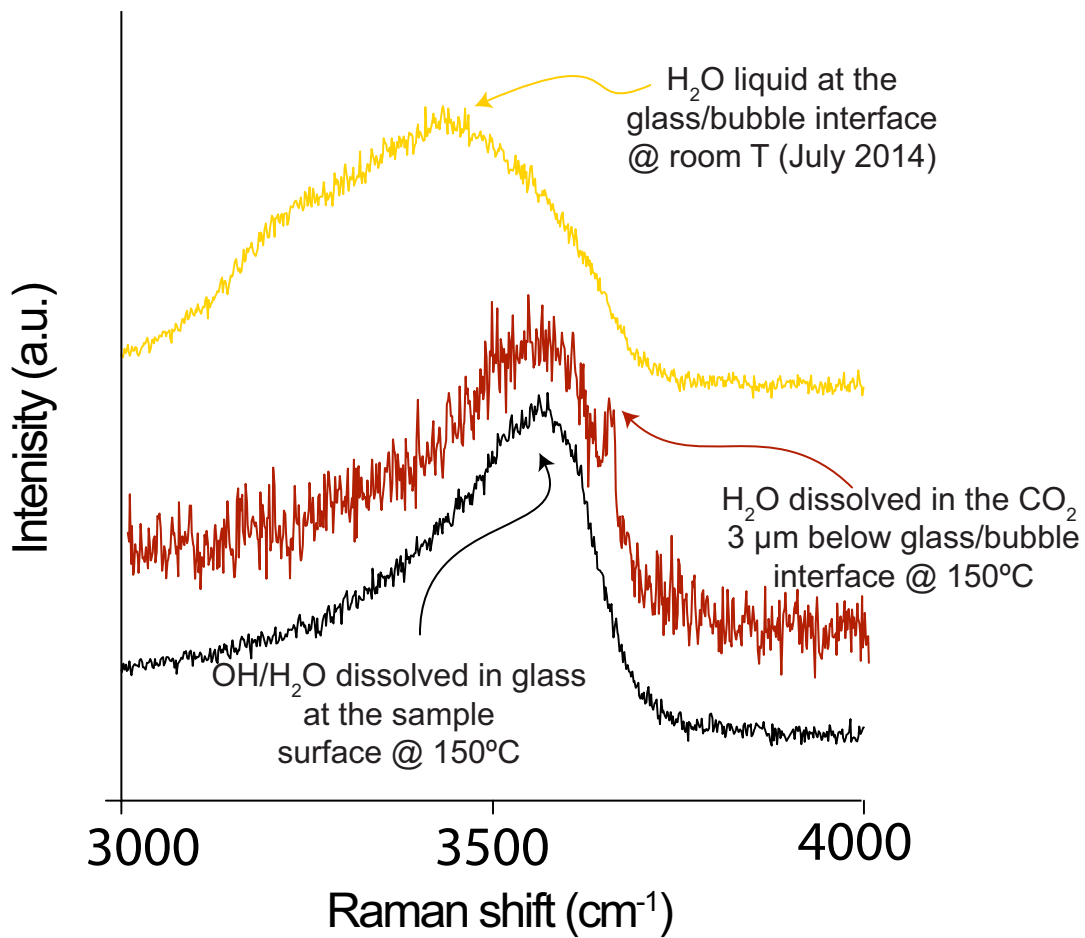


Fig. 3